

Original Research

Combined HASPIN and mTOR inhibition is synergistic against KRAS-driven carcinomas

Chenyue Xu^{a,b,1}, Qiongmei Gao^{c,1}, Zhengming Wu^d, Weijuan Lou^e, Xiaoyan Li^f,
Menghui Wang^b, Nianhong Wang^{g,*}, Qingquan Li^{b,*}

^a Department of Pathology, School of Basic Medical Sciences, Fudan University, Shanghai 200032, China

^b Department of Pharmacology, School of Pharmacy, Fudan University, Shanghai 201203, China

^c Department of Endocrinology and Metabolism, Shanghai Jiao Tong University Affiliated Sixth People's Hospital, Shanghai Key Laboratory of Diabetes Mellitus, Shanghai Clinical Center of Diabetes, Shanghai 200233, China

^d Department of Pharmacology and Moores Cancer Center, University of California San Diego, La Jolla, CA 92093, USA

^e Department of Nephrology, Shanghai Fourth People's Hospital, School of Medicine, Tongji University, Shanghai 200434, China

^f Department of General Surgery, Huashan Hospital, Fudan University, Shanghai 200040, China

^g Department of Rehabilitation Medicine, Huashan Hospital, Fudan University, Shanghai 200040, China

ARTICLE INFO

Keywords:

KRAS
HASPIN
mTOR
VRK1
Cancer

ABSTRACT

Background: Oncogenic mutations in the KRAS gene are very common in human cancers, resulting in cells with well-characterized selective advantages. For more than three decades, the development of effective therapeutics to inhibit KRAS-driven tumorigenesis has proved a formidable challenge and KRAS was considered 'undrug-gable'. Therefore, multi-targeted therapy may provide a reasonable strategy for the effective treatment of KRAS-driven cancers. Here, we assess the efficacy and mechanistic rationale for combining HASPIN and mTOR inhibition as a potential therapy for cancers carrying KRAS mutations.

Methods: We investigated the synergistic effect of a combination of mTOR and HASPIN inhibitors on cell viability, cell cycle, cell apoptosis, DNA damage, and mitotic catastrophe using a panel of human KRAS-mutant and wild-type tumor cell lines. Subsequently, the human transplant models were used to test the therapeutic efficacy and pharmacodynamic effects of the dual therapy.

Results: We demonstrated that the combination of mTOR and HASPIN inhibitors induced potent synergistic cytotoxic effects in KRAS-mutant cell lines and delayed the growth of human tumor xenograft. Mechanistically, we showed that inhibiting of mTOR potentiates HASPIN inhibition by preventing the phosphorylation of H3 histones, exacerbating mitotic catastrophe and DNA damage in tumor cell lines with KRAS mutations, and this effect is due in part to a reduction in VRK1.

Conclusions: These findings indicate that increased DNA damage and mitotic catastrophe are the basis for the effective synergistic effect observed with mTOR and HASPIN inhibition, and support the clinical evaluation of this dual therapy in patients with KRAS-mutant tumors.

Introduction

KRAS mutations occur in approximately 30% of tumors, making it

one of the most common genetic mutations associated with cancer. They are frequent triggers for lung, colorectal and pancreatic cancers. KRAS is mutated in 32% of lung cancers, 40% of colorectal cancers (CRC), and

Abbreviation: CPC, Chromosome passenger complex; CCK8, Cell-Counting kit 8; cPARP, cleaved PARP; DDR, DNA damage response; H&E, Hematoxylin and eosin; HASPIN, Haploid Germ Cell-Specific Nuclear Protein Kinase; H3T3ph, Kinase that phosphorylates histone H3 at threonine 3; IHC, Immunohistochemistry; KRAS-WT, KRAS-wildtype; KRAS-Mut, KRAS-mutant; KO, Knockout; mTOR, Mammalian target to rapamycin; MC, Mitotic catastrophe; OE, Overexpression; PDAC, Pancreatic ductal adenocarcinoma; PFS, Progression-free survival; PTX, Paclitaxel; TNBC, Triple-negative breast cancer; TUNEL, Terminal deoxynucleotidyl transferase dUTP nick end labeling; VRK1, Vaccinia-related kinase 1.

* Corresponding authors.

E-mail addresses: wnh@fudan.edu.cn (N. Wang), 061101040@fudan.edu.cn (Q. Li).

¹ Contributed equally.

<https://doi.org/10.1016/j.tranon.2022.101540>

Received 9 June 2022; Received in revised form 16 August 2022; Accepted 7 September 2022

1936-5233/© 2022 The Authors. Published by Elsevier Inc. This is an open access article under the CC BY-NC-ND license (<http://creativecommons.org/licenses/by-nc-nd/4.0/>).

90% of pancreatic ductal cancers (PDAC) [1]. KRAS remains a pharmacologic challenge in direct inhibition due to its structure as well as picomolar affinity to GDP/GTP, except for recent advances in selective inhibitors targeting the G12C variant with AMG 510 [2–6]. Patients with tumors harboring KRAS mutations are among the most difficult to treat. Individual inhibitors targeting mutated RAS downstream signaling pathways (such as PI3K/AKT/mTOR and RAF/MEK/ERK, etc) have achieved limited response rates of less than 20% in clinical trials [7]. This suggests that RAS is related to cascading crosstalk of signals that leads to a high degree of complexity and redundancy in bypass pathways and negative feedback loops [8]. Given the greater molecular diversity of tumors with KRAS mutations compared with other operable oncogenic targets in tumors, one way to improve the clinical efficacy of inhibitors is to identify drug combinations that either target multiple RAS-driven pathways or circumvent resistance.

mTOR (Mammalian target to rapamycin) is a critical downstream effector of KRAS and plays an important role in the occurrence and development of a variety of tumors [9]. The hyper-activated mTOR pathway is a characteristic hallmark after chemotherapy in KRAS-mutant lung adenocarcinoma and mTOR inhibition circumvents the refractory phenotype and restored the sensitivity of drug-resistant KRAS mutated lung cancer cells to chemotherapy [10]. In pancreatic ductal adenocarcinoma, KRAS remains a difficult target to suppress pharmacologically [11–13]. Pharmacological inhibition of mutation-activated KRAS or MEK leads to rapid adaptive activation of mTORC1/2 pathways, leading to tumor regeneration after initial regression. A combined approach of co-targeting KRAS or MEK and mTORC1/2 complexes to overcome adaptive responses and achieve sustained PDAC tumor growth inhibition [14]. Clinical trials of mTOR inhibitors in colorectal cancer with high KRAS activation rates have been investigated in CRC [15]. mTOR inhibitors may represent an attractive anti-tumor target, combined with strategies to target other pathways that may overcome resistance [9,16–18]. Although mTOR inhibitors have been widely used in clinical studies, there is limited efficacy in treating tumors with mTOR inhibitors alone in KRAS mutated tumors. In KRAS-mutant lung cancer, the mTOR inhibitor Ridaforolimus as a monotherapy showed little clinical benefit in a phase II trial, resulting in only a modest increase in PFS (Progression-free survival) [19]. Likewise, early phase II studies of mTOR inhibition alone in KRAS-dependent PDAC subtypes showed no improvement in overall survival [13]. In KRAS-mutant metastatic colorectal cancer, the mTOR inhibitor temsirolimus (CCI-779) or everolimus alone has no significant anti-tumor activity in phase II studies [20–22]. Therefore, it is particularly important to find synergistic lethal targets of mTOR inhibitor for KRAS-mutant tumors.

HASPIN (Haploid Germ Cell-Specific Nuclear Protein Kinase) is a recently discovered mitotic kinase that phosphorylates histone H3 at threonine 3 (H3-T3). Phosphorylation of H3-T3 promotes inner centromeric localization of the chromosome passenger complex (CPC) during mitosis and is essential for the function of Aurora B at the centromere [23–25]. Consumption of HASPIN by siRNA results in defective mitosis, characterized by chromosome misalignment, premature loss of cohesion between sister chromatids, and the formation of multipolar spindles [26]. mTOR plays an important role in the normal mitosis of cells. The report has shown that Mio (a highly conserved member of the SEACAT/GATOR2 complex) possibly by linking Plk1 and Aurora A to mTOR signaling in a pathway to promote faithful mitotic progression in HeLa cells. Reduced mTOR activity causes the mitotic defects observed upon Mio depletion [27]. mTORC1 cooperates with nuclear RNAPII-CTD kinase CDK12 through phosphorylation of 4E-BP1, and plays a vital role in maintaining the stability of mitotic chromosomes [28]. Although previous studies have shown that HASPIN inhibitors such as CHR-6494, augment the effects of chemotherapy by driving transformed cells to mitotic catastrophe [29], it is unclear whether HASPIN inhibition potentiates the effects of mTOR.

Here, we investigated the mechanism underlying KRAS-mutant cell

sensitivity to dual HASPIN and mTOR inhibition. We show that HASPIN inhibition in KRAS-mutant cells induces mitotic catastrophe accumulation, which is further compounded by simultaneous preventing phosphorylation of histone H3, mediated by mTOR inhibition. Importantly, intraperitoneal administration of mTOR and HASPIN inhibitors at clinically relevant doses caused a significant reduction in human xenografted tumor growth. Our results support further clinical investigation of combined HASPIN/mTOR inhibition as a potential KRAS-driven carcinomas therapy.

Materials and methods

Cell lines and reagents

Human tumor cell lines HCT116, A549, LOVO, SW480, SW620, HPAF-II, MDA-MB-231, HT29, BXP3, H446, and H1688 were purchased from the American Type Culture Collection (ATCC). Each tumor cell line was cultured in its standard medium as recommended by the ATCC. Human embryonic kidney 293T (HEK293T) cells were cultured in DMEM medium supplemented with 10% FBS and antibiotics. All cells were cultivated at standard tissue culture conditions (37°C and 5% CO₂/95% air). Fresh medium was added every 2 to 3 days. For in vitro studies, the HASPIN inhibitor (CHR-6494) and mTOR inhibitor (CCI-779) were ordered from MCE (MedChem Express, Shanghai, China), and dissolved in dimethyl sulfoxide (DMSO).

Stable cell pools generation

Vectors cloned with cDNA of KRAS-G12V, Flag-Aurora B, and Flag-Survivin, and sgRNA targeting VRK1 were constructed. Retroviral or lentiviral expressing systems were used to generate stable overexpression or knockout cell lines. cDNA encoding Flag-Aurora B and Flag-Survivin were cloned into pCDH (Supplemental Methods). KRAS-G12V cDNA was cloned into pBABE (Addgene, #46746). sgRNAs targeting VRK1 and HASPIN were designed using CHOPCHOP (<https://chopchop.rc.fas.harvard.edu>) and cloned into LentiCRISPRv2 vector (Addgene, #52961) digested with BsmB1 and ligated with annealed oligonucleotides acid. In brief, retrovirus particles were produced in HEK293T cells using Polyethylenimine (PEI) (Beyotime, Shanghai, China) transfection. Lentiviruses were prepared by transfecting two packaging plasmids into HEK293T cells using PolyJet (SigmaGen; Shandong, China). After filtration with a Millex-HV sterile 0.45µm filter (Merck Millipore, Shanghai, China) and titration, viruses were added to cells in presence of polybrene (10µgml⁻¹). The medium was replaced 24–48h after infection, followed by selection with puromycin (5µgml⁻¹) for 1–2 weeks. Protein overexpression or knockdown efficiency was confirmed by quantitative real-time PCR or western blot. The VRK1 knockout target sequences are as follows: 5'-CACGACGAGCATC-GATGCACACAA-3'. The HASPIN knockout target sequences are as follows: sgRNA1 5'-CACCGCTTAGCAAATACATAGAGG-3' and sgRNA2 5'-CACCGTGCACACTTCACCGATAAG-3'

Proliferation and colony formation

Cell proliferation was measured by using the Cell-Counting kit 8 (CCK8) assay. Cells were seeded in 96-well plates (1,000 cells/ well) with 10% FBS in culture medium, and treated with indicated agents for 72 h. CCK8 (Dojindo Molecular Technologies, Rockville, USA) was added to the wells prior to incubation for 2 h at 37°C. The assay was performed according to the manufacturer's instructions. Cell viability of the treated group was normalized to the vehicle control. IC50 values were determined using the Prism 7 Software (LaJolla, California, USA). The combination indices (CI) were calculated by CompuSyn software using the Chou-Talalay method (Biosoft, Palo Alto, CA); additive effect (CI=1), synergism (CI<1), and antagonism (CI>1) [30].

For colony formation assays, cells were seeded in triplicate in 6-well

dishes (1,000 cells/well) and allowed to adhere overnight in culture media. The cells were then cultured with the drug(s) alone or in combination, or with the vehicle in complete media for 14 days. Observed colonies were fixed with 0.4% buffered paraformaldehyde and then stained with crystal violet for 20 min. The colonies were enumerated using Image J software (NIH, Maryland, USA). Image J filters scored colonies that were $\geq 100\mu\text{m}$ in size.

Human xenograft models

BALB/C nude male mice, aged 4–5 weeks, were obtained from Shanghai Slack Laboratory Animal Co. Ltd (Shanghai, China). Animals were maintained in a sterile environment; their cages, food, and bedding were sterilized by autoclaving. All manipulations were performed under sterile conditions following procedures approved by the Experimental Animal Management and Ethics Committee of University. A549 (1×10^7), HCT116 (7.5×10^6), HPAF-II (1×10^7) was injected subcutaneously in the flanks of all experimental nude mice. For treatment, mice were randomized into 4 groups ($n = 5-6$ per group) with similar mean tumor volumes of approximately $40-50 \text{ mm}^3$. Mice were treated with vehicle, 50 mg/kg CHR-6494 (in 0.5% Sodium carboxymethyl cellulose), 20 mg/kg CCI-779 (in 0.5% Sodium carboxymethyl cellulose), or a combination of CHR-6494 and CCI-779 via intraperitoneal injection.

MDA-MB-231 (5×10^6) cells were injected subcutaneously in each animal. 25 tumor-bearing mice (50 mm^3 tumor volume) were randomized into five groups and exposed to vehicle, 50 mg/kg CHR-6494, 20 mg/kg CCI-779 or CHR-6494/CCI-779 in combination via intraperitoneal injection in four cycles of three consecutive days for 21 days, or 20 mg/kg paclitaxel (in 0.5% Sodium carboxymethyl cellulose) (MedChem Express, Shanghai, China) via intraperitoneal injection for every other day.

Tumor growth was measured every 3 days using a digital caliper and volume was assessed as $(\text{length} \times \text{width}^2)/2$. Bodyweight was measured every 3 days as an indicator of toxicity. Mice were euthanized when the tumor volume reached the best contrast effect. At sacrifice, tumors were excised and weighted. Upon killing mice, portions of tumors were snap-frozen and stored in liquid nitrogen or were fixed in 10% buffered formalin for routine histopathologic processing.

Western blot analyses and antibodies

Total cell lysates were prepared from the cells after treatment with the drug(s) or vehicle with RIPA Buffer (Beyotime, China) supplemented with protease and phosphatase inhibitor cocktail (Roche) and 1% sodium dodecyl sulfate (SDS). The protein concentration was determined using the Pierce BCA assay kit solution (Thermo Fisher Scientific, Waltham, USA). An equal amount of proteins was resolved by electrophoresis on 10% SDS-PAGE gradient gels and transferred to PVDF membranes, blocked for 1 h at room temperature with 5% milk in TBST and the membranes were probed with primary antibodies in 5% BSA overnight. Primary antibodies included: cPARP (Cell Signaling, #9541), phospho-histone H2AX (Ser 139) (20E3, #9718), pCDK1^{Y15} (10A11, #4539), CHK2 (D9C6) (#6334), Phospho-CHK2 (Thr68) (C13C1, #2197), Phospho-p53 (Ser 20) (#9287), Survivin (#2808), Flag Tag (#14793), p53 (sc-126, Santa Cruz,); CDK1 (Santa Cruz, sc-54,); Aurora B (Santa Cruz, sc-393357) Histone H3 (Proteintech, 17168-1-AP). After washing, the membranes were probed with Anti-rabbit IgG (Proteintech, SA00001-2) or Anti-mouse IgG (Proteintech, SA00001-1) HRP-linked secondary antibodies. Bands were visualized using chemiluminescence (Western chemiluminescence HRP Substrate, Millipore, Boston, USA) on an image reader BIO-RAD ChemiDoc Imaging System (BIO-RAD, Shanghai, China). Equal protein loading was assessed using GAPDH (Abcam, ab128915) or Vinculin (Abcam, ab129002) antibodies.

Quantitative real-time PCR

Total RNA was extracted from A549 and SW480 cells with RNA Isolation Kit (Vazyme, Shanghai, China). cDNA was synthesized by a reverse transcription kit (Vazyme, China). Amplification was performed with iTaq Universal SYBR Green Supermix (BIO-RAD, China) under universal cycling conditions using the ABI 7500 system (Applied Biosystems, CA, UAS). Relative mRNA expression was calculated using the $2^{-\Delta\Delta\text{Ct}}$ method. GAPDH was used as the housekeeping gene. The primer sequences were as follows: VRK1 (forward, 5'-CCTCGTGTAAGCAGCTCAA-3'; reverse, 5'-GCCAATGGGTAATCC-TACTTCC-3'), KRAS (forward, 5'-GCAAGAGTGCCTTGACGATA-3'; reverse, 5'-CCCTCATTGCACTGTACTCC-3') and GAPDH (forward, 5'-GGAGCGAGATCCCTCCAAAAT-3'; reverse, 5'-GGCTGTTGTCA-TACTTCTCATGG-3').

Immunohistochemistry (IHC)

Tissues were fixed with 10% buffered formalin at 4°C for overnight and embedded in paraffin (FFPE). FFPE were sectioned at 4- μm thickness. For IHC staining, tissue sections were deparaffinized and rehydrated, endogenous peroxidase activity was quenched by incubating the sections in a 3% hydrogen peroxide (H₂O₂)-methanol solution for 30 min at room temperature. Antigen retrieval was then subjected to 0.01 M citrate buffer (pH 6.0) for 13 min at high temperature (95-100°C). Tissues were blocked with 10% normal goat serum (Abcam, Cambridge, UK) in phosphate-buffered saline (PBS) for 20 min at room temperature. Primary antibodies against Ki-67 (Abcam, ab16667) and γ -H2AX (Cell Signaling, #9718) were used for staining following dilution in antibody diluent. HRP-conjugated secondary antibodies were used, and followed by DAB Chromogen staining using rabbit/mouse peroxidase/3, 3'-diaminobenzidine (DAB) EnVision™ Detection kit (Agilent-Dako, California, UAS). Tissue sections were counterstained with hematoxylin to show cell nuclei. Five fields per tumor section were quantified using Image J software for Ki-67 or γ -H2AX-positive cell staining with a minimum sample size of 5 animals per cohort.

TUNEL and H&E staining

TUNEL staining was performed on paraffin sections using the ApopTag® Peroxidase In Situ Apoptosis Detection Kit (Millipore, #S7100). TUNEL-positive cell staining was quantified in 5 regions of each tumor section using Image J software with a minimum sample size of 5 animals per cohort. Hematoxylin and eosin (H&E) staining was done by standard techniques.

Immunofluorescence staining

Cells were placed on the slides treated with the indicated concentrations for 72 h and followed fixation with 4% paraformaldehyde in PBS for 20 min at room temperature, permeabilized with 5% Triton X-100 in PBS for 30 min. Blocked cells with 3% bovine serum albumin (BSA) were incubated with primary antibodies γ -H2AX (Cell Signaling, #9718), p-Aurora A/B/C (Cell Signaling, # 2914), Survivin (Cell Signaling, #2808), Aurora B (Santa Cruz, sc-393357), or ACA (ImmunoVision, HCT-0100) in a humidity chamber overnight. The slides were then incubated with Alexa Fluor 488 fluorochrome-conjugated secondary antibodies (Abcam, ab150077) or Alexa Fluor 647 fluorochrome-conjugated secondary antibodies (Invitrogen, A-21445) for 1h at room temperature. Stained cells were mounted with DAPI (Beyotime, China). The Nikon microscope was used to image the fluorescently-stained slides and analysis. We acquired a range of 10–20 fields per treatment using oil 100x objective magnification and at least 120 cells were analyzed using Image J software for data analysis.

Flow cytometric analysis for cell cycle and apoptosis

A549 and HCT116 cells were treated with CHR-6494 (600 nM) and/or CCI-779 (3 μ M) for 72 h. Floating and trypsin-detached cells (1×10^6) were collected and fixed in 70% cold ethanol for 2 hr. Subsequently, the cells were washed once with PBS, resuspended in PBS containing 200 mg/ml RNase A, incubated at 37°C for 30 min, and stained with 50 mg/ml propidium iodide (PI, BD Biosciences, New Jersey, UAS). Cell cycle distribution was acquired by BD LSRFortessa flow cytometry (BD Biosciences, USA), and the data were analyzed using ModFit LT software (TreeStar, Ashland, OR).

To assess apoptotic cell death, we prepared A549 and HCT116 cells as described above. The cells were collected and then stained with 5 μ l Annexin V-FITC and 5 μ l 7AAD-PI (YEASEN, Shanghai, China) according to the manufacturer's instructions for adherent cells. Finally, Stained cells were analyzed using a BD LSRFortessa flow cytometer (BD Biosciences, USA), with FlowJO 10 software used for data analysis.

Statistical analysis

All statistical analysis was performed using GraphPad Prism 7 (La Jolla, California, CA) software. Results are expressed as mean \pm SD of the indicated number of independent experiments. The P values were calculated using the Student t-test for comparison of two groups. For multiple comparisons, two-way ANOVA was performed. P values of < 0.05 were considered statistically significant.

Results

Inhibition of HASPIN sensitized KRAS-mutant cancer cell lines to mTOR inhibitor treatment in vitro

We first evaluated the effect of combination treatment with HASPIN inhibitor (CHR-6494) and mTOR inhibitor (CCI-779) to inhibit cell proliferation of a panel of KRAS-mutant (A549, SW480, SW620, HPAF-II, LOVO, and HCT116) and KRAS-wildtype (HT29, BXP3, H446, and H1688) cell lines (Fig. 1A-1C, Supplementary Table 1). The proliferation assay showed the drugs affected all the KRAS-mutant cell lines tested, both single agents and in combination after 72 h' treatment (Fig. 1A). However, all cell lines were more sensitive to combination treatment compared to single therapy (Fig. 1A). Synergism was determined by the combination indices (CI) calculated using the Chou-Talalay method [30]. Strikingly, the combination indices analysis demonstrated that dual inhibition of HASPIN and mTOR synergistically suppressed cell viability of all KRAS-mutant cells (Fig. 1B). The synergistic cell suppressing we observed with HASPIN and mTOR inhibitor is unlikely due to off-target effects because knockout of HASPIN with sgRNA shows cooperative inhibition as well (Supplementary Fig. 1). In contrast, no stronger inhibitory activity was observed in any of the KRAS-wildtype cell lines treated with the drug combination, compared to the single-agent (Fig. 1C). IC50 values for CHR-6494 and CCI-779 were established (Supplementary Table 2). These results suggested that the two targeted drugs may have a complementary mechanism of action in KRAS-mutant cell lines.

Further evaluation of the colony growth ability of KRAS-mutant cells (A549 and HPAF-II) and KRAS-wildtype cells (HT29 and H446) under long-term treatment showed that compared with monotherapy or vehicle control, the colony formation of dual inhibitory treatment was significantly reduced in KRAS-mutant but not in KRAS-wildtype cells (Fig. 1D-H). Taken together, the combinatorial inhibition of HASPIN and mTOR was synergistically superior to either single drug in inhibition of cell viability and anchorage-dependent growth in KRAS-mutant cells.

Antitumor activity of combination treatment in human KRAS-driven tumor xenografted models

Given the biological implications of our in vitro data, we further explored the combinatorial anti-tumor activity of CHR-6494 and CCI-779 in HCT116 and A549 cells xenografted in vivo mouse models. According to the aforementioned animal experiment protocol and schematic depiction of Fig. 2A, when the tumor reached 40-50mm³, HCT116 or A549 tumor-bearing mice were grouped (n=5) and administered i.p. with CHR-6494, CCI-779 or combination treatment. In HCT116 xenografts, although no tumor completed regression was observed in any groups with different treatment, tumor growth was significantly retarded in the group with combined CHR-6494 and CCI-779, with essentially no increase in tumor size (Fig. 2B-2C). Combination treatment for 27 days suppressed tumor progression (baseline 56.2 \pm 20 mm³, post-treatment 77 \pm 35 mm³), whereas the vehicle-treated tumors progressed from 58 \pm 24 to 1460 \pm 56 mm³ (Fig. 2C). At the time of sacrifice, tumors treated with the combination weighed nearly 97% less than the vehicle-treated group (Fig. 2D). As seen before, CHR-6494 and CCI-779 single treatment led to tumor growth delay, but combined treatment led to tumor shrinkage in mice bearing A549 xenografts (Fig. 2E-F). At the endpoint, tumors treated with the combination weighed significantly lower on average than vehicle-treated tumors (Fig. 2G). To further verify the efficacy of combination therapy, we expanded the type of KRAS mutant HPAF-II cancer cells xenografted mice models. Consistent with the antitumor effect of the combination in the HCT116 and A549 xenograft model, we observed similar effects on tumor size, tumor growth, and tumor weight in HPAF-II xenografts as well (Supplementary Fig. 2A-2C).

To evaluate the ability of combined therapy to induce apoptosis and DNA damage in vivo, cells staining positively for the DNA fragmentation marker TUNEL (Terminal deoxynucleotidyl transferase dUTP nick end labeling) and the DNA damage marker γ -H2AX were quantified in HCT116 tumors after combined treatment and compared to vehicle controls (Fig. 2H-2K). We detected significantly increased numbers of TUNEL and γ -H2AX-positive tumor cells in the combination-treated tumors compared to controls (Fig. 2H-2I and 2K). It also reduces the fraction of proliferating tumor cells, as measured by Ki-67 staining (Fig. 2H and 2J). Histological evaluation of HPAF-II dissected tumor, the same results as HCT116 xenograft were obtained (Supplementary Fig. 2D-2G). To further verify the ability of combined treatment to induce both apoptotic and DNA damage response in vivo, xenograft-bearing mice were treated for 72 h. Western blot analysis showed an increase in γ -H2AX and levels of cleaved PARP (cPARP) (Fig. 2L). Of note, monotherapy with either CHR-6494 and CCI-779 alone failed to induce significant detectable accumulation of γ -H2AX or cleaved PARP (Fig. 2L).

Combination treatment with HASPIN and mTOR inhibitors leads to mitotic catastrophe in cells by preventing H3 phosphorylation

Given the potent in vitro and in vivo treatment response, we next examined downstream effectors of HASPIN and mTOR inhibition. We found that treated with HASPIN or mTOR inhibitor alone in A549 cells, the phosphorylation level of H3 histones in Thr3 (H3T3ph) was slightly reduced, or even negligible, compared with the significant reduction in combination therapy (Fig. 3A). Consistent with this finding in SW480 cells, the combined treatment strongly suppressed the phosphorylation of histone H3 (Fig. 3A).

Aurora B forms a complex with a histone H3, which has been phosphorylated in Thr3, and this binding of AURKB is mediated by Survivin [31]. Insufficient H3 phosphorylation sites will prevent chromosomal passenger complex (CPC) binding to histones [32]. Thus, we next confirmed that combination therapy resulted in the loss of Survivin and Aurora B interaction with H3 without any effect on the expression of the total CPC (Aurora B and Survivin) protein in nocodazole-treated

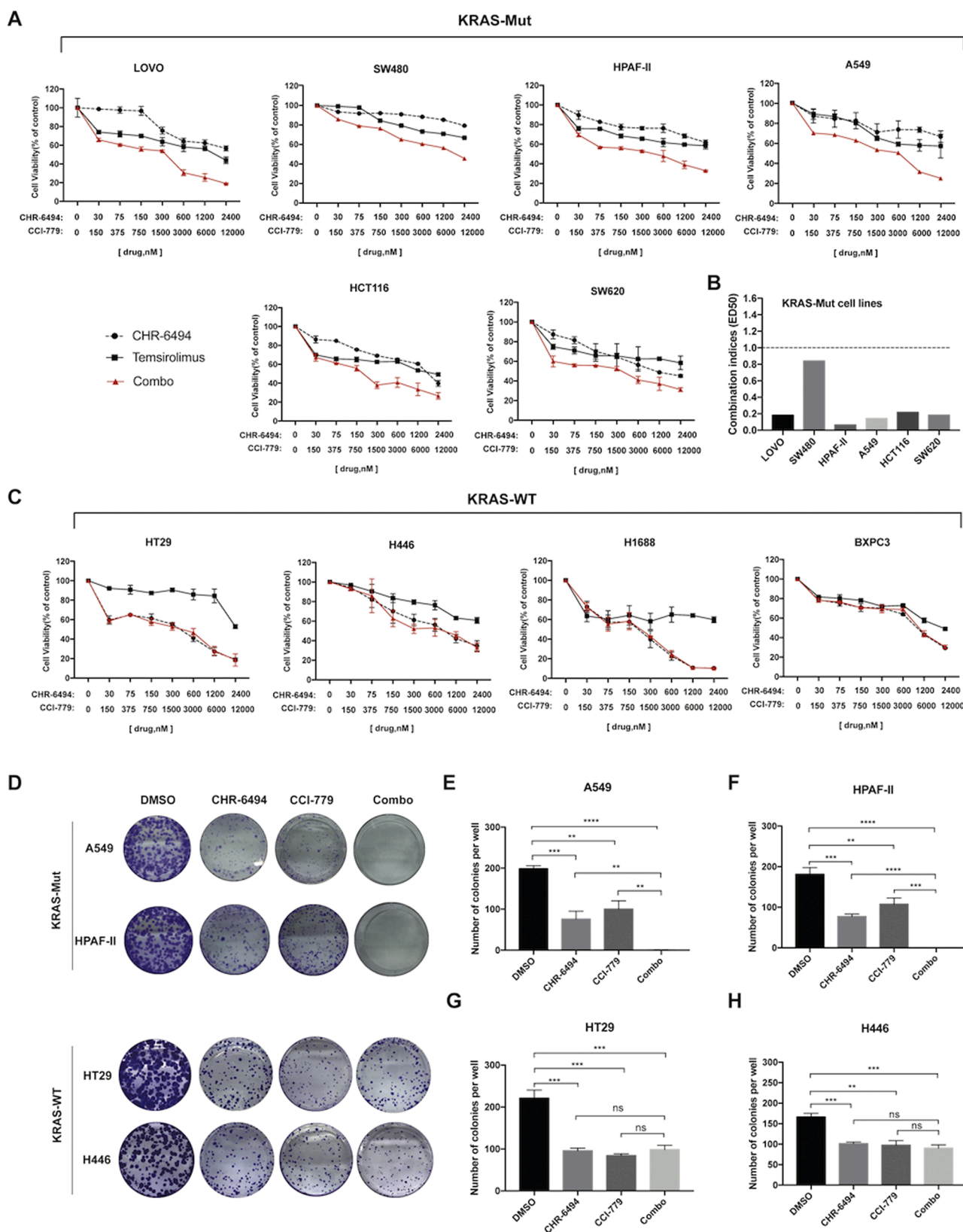
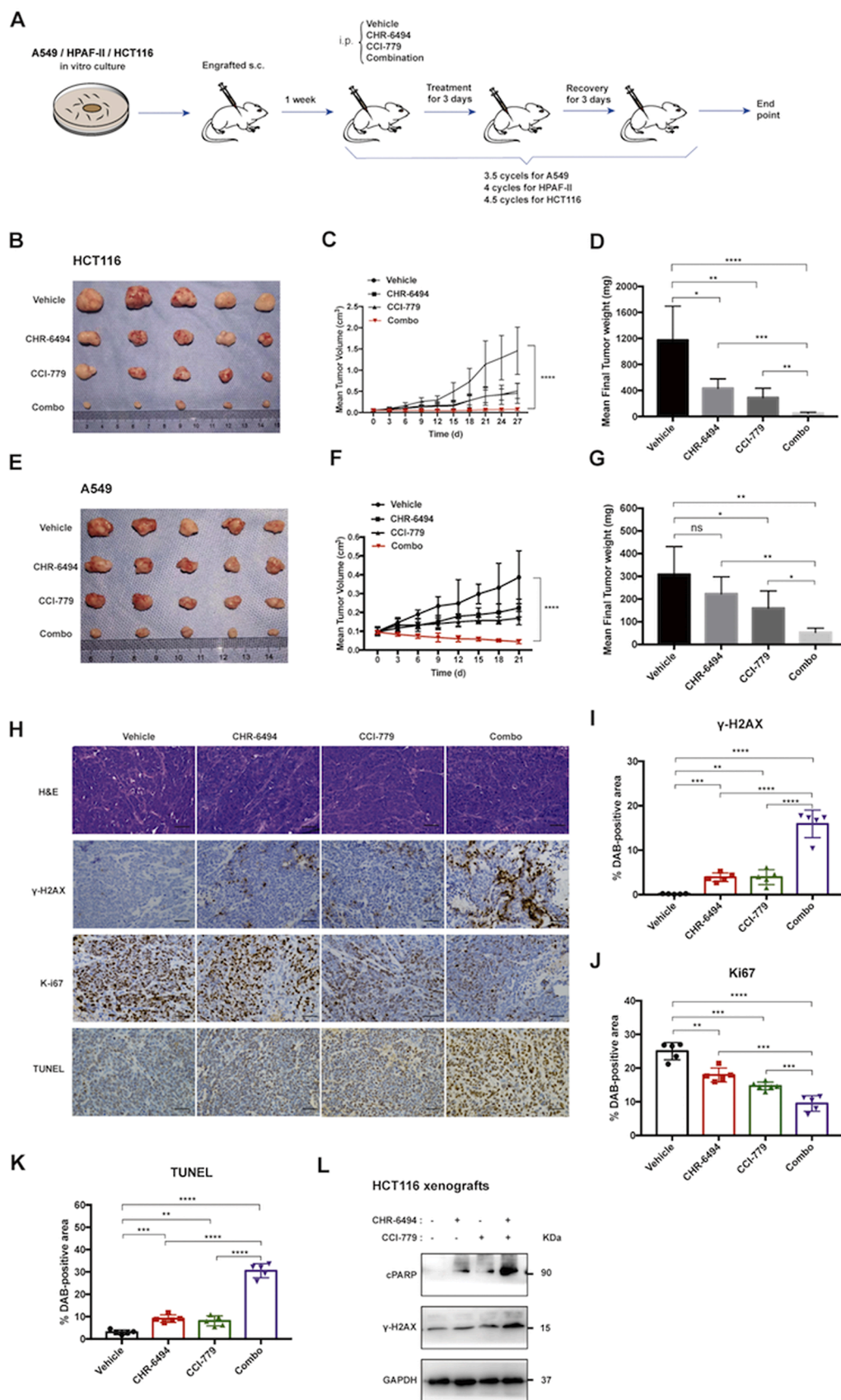


Fig. 1. Inhibition of HASPIN sensitized KRAS-mutant cancer cell lines to mTOR inhibitor treatment in vitro.

(A–C) Synergistic interaction between HASPIN inhibitor (CHR-6494) and mTOR inhibitor (CCI-779) was measured. (A) KRAS-mutant (KRAS-Mut) tumor cell lines were treated with CHR-6494 (600nM) or/and CCI-779 for 72 h. (B) CompuSyn combination indices (CI) were derived from seven-point concentration proliferation experiments. The cutoff for additive effect (CI: 1) is marked by a dashed line. (C) KRAS-wildtype (KRAS-WT) tumor cell lines were treated for three days with either single agents or combined agents. (D) Representative images of KRAS-Mut tumor cell lines (A549 and HPAF-II) and KRAS-WT tumor cell lines (HT29 and H446) colony formation, untreated or treated with either CHR-6494 (600nM), CCI-779 (3 μ M), or in combination for 2 weeks. (E–H) Mean number of colonies formed after treating cells for 2 weeks. Data represent mean \pm SD (n=3). ns: not significant, * p < 0.05, ** p < 0.01, *** p < 0.001, and **** p < 0.0001.



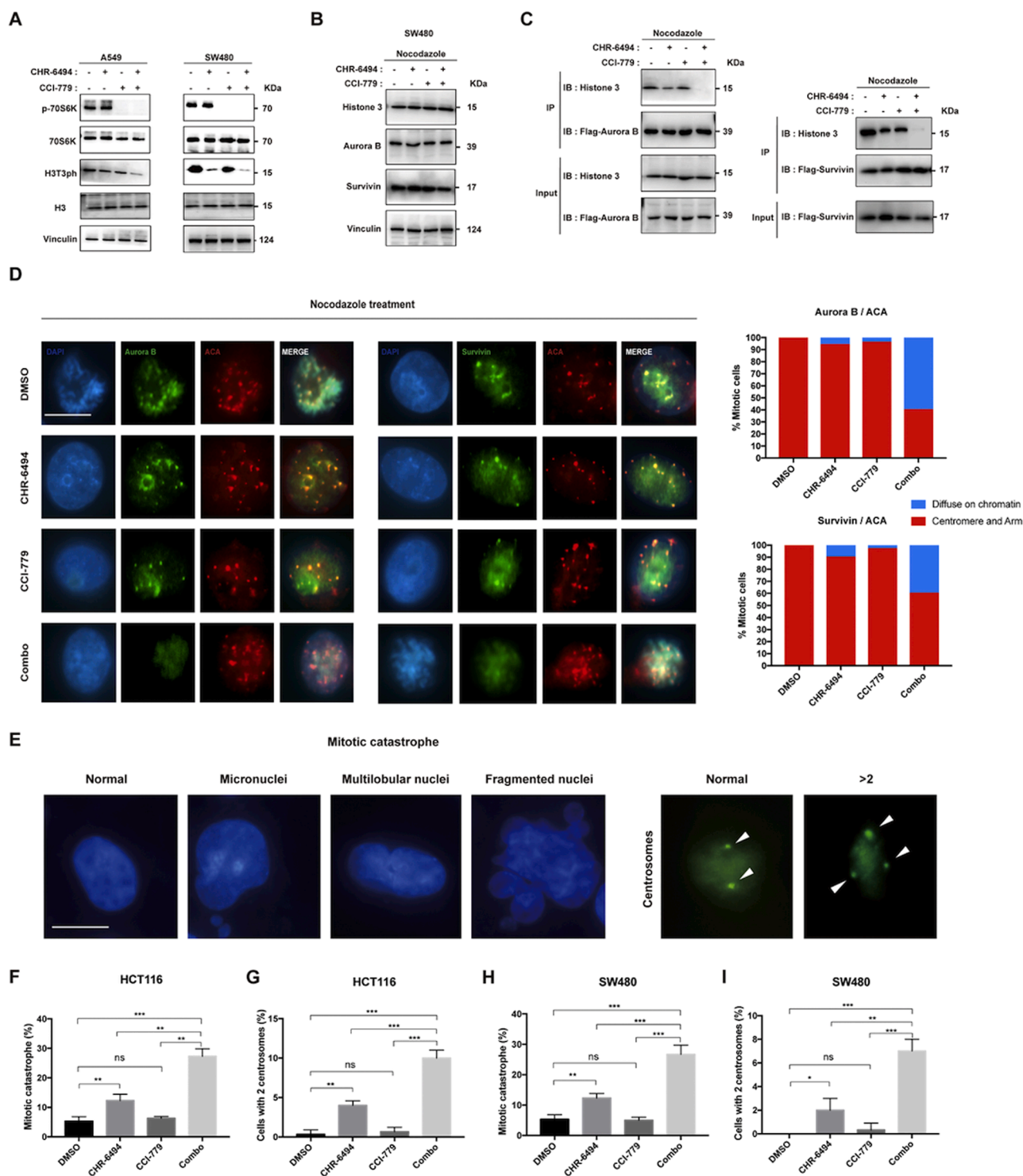


Fig. 3. Combination treatment with HSPIN and mTOR inhibitors leads to mitotic catastrophe in cells by preventing H3 phosphorylation.

(A) Representative western blots showing protein levels of downstream target engagement (H3T3ph and p70S6K) in A549 and SW480 cells treated for 72 h with DMSO, CHR-6494 (600nM), CCI-779 (3 μ M), or combination. (B) SW480 cells were synchronized and treated with indicated drugs for 72 h and harvested in mitosis by mechanical shake-off. Western blots showing CPC protein levels (Aurora B and Survivin) and total Histone 3 levels. (C) Immunoblot analysis of the strength of the interaction between CPC protein (Aurora B and Survivin) and Histone 3 with immunoprecipitated equal protein of Flag-aurora B (left) and Flag-Survivin (right) after 72 h treatment with either 600nM CHR-6494, 3 μ M CCI-779, or both in nocodazole-treated SW480 cells. (D) SW480 cells were synchronized and exposed to indicated drugs for 72h. The level of CPC protein concentration on centromeres was analyzed by immunofluorescence. The quantification of the CPC and ACA signals, and the DAPI signal (DNA) were quantified and their overlap is shown in the graphs below. A total of 100 cells were counted taking into account the distribution of CPC on centromeres and chromosome arm or spread on the chromatin. Scale bar: 10 μ m. (E) SW480 cells with features of mitotic catastrophe (MC), such as micronuclei, multilobular, fragmented nuclei (left), and containing >2 centrosomes (right) treated with the indicated drug singly or in combination for 72 h. Scale bar: 10 μ m. (F and G) MC and abnormal centrosome amplification were quantitated to HCT116 cells. (H and I) MC and abnormal centrosome amplification were quantitated to SW480 cells. Data are expressed as means \pm SD (n=3) of the three experiments, ns: not significant, * p < 0.05, ** p < 0.01, *** p < 0.001.

synchronized SW480 cells (Fig. 3B-3C). The expression of H3T3ph is required for the recruitment of CPC to centromeres in mitosis to perform normal mitotic regulation functions [23]. In this context, we examined the colocalization of ACA (anti-centromere antibody) and CPC on centromeres in SW480 cells treated with single agents or the combination by immunofluorescence. Control-treated cells displayed a typical localization of ACA and CPC, whereas slight delocalization of CPC protein on ACA was observed in single-treated cells (Fig. 3D). Moreover, the combination treatment of CHR-6494 and CCI-779 resulted in dramatically delocalization of CPC proteins (Fig. 3D). Furthermore, we examined the effect of indicated drugs treatment on mitotic catastrophe. Compared to control and CCI-779 treatment, in CHR-6494-treated SW480 and HCT116 cells, DAPI staining cell nuclei and immunostaining with p-Aurora A/B/C displayed an increased number of cells with features of mitotic catastrophe (MC) such as micronuclei, multilobular nuclei, and fragmented nuclei, and cells containing more than two centrosomes, respectively (Fig. 3F-3I). Typical microphotographs were

shown in Fig. 3e. Interestingly, quantitative analysis showed that the number of cells having the characteristics of MC was significantly increased at dual treatment in SW480 (Fig. 3F) and HCT116 cells (Fig. 3H). On the other hand, cells containing more than two centrosomes were also highly increased after combination therapy in SW480 cells (Fig. 3G) and HCT116 cells (Fig. 3I). Together, these results indicate that the HASPIN and mTOR have a synergistic effect on molecular functions to affect the process of cell mitosis by regulating the phosphorylation of histone H3.

On-target inhibition of HASPIN and mTOR synergistically trigger enhanced DNA damage and apoptosis in KRAS-mutant cells

Mitotic catastrophe is an important mechanism for the death of cancer cells induced by anti-neoplastic agents that damage DNA [33]. Given that the combinatorial inhibition of HASPIN and mTOR resulted in much greater abnormal mitoses compared to either control or single

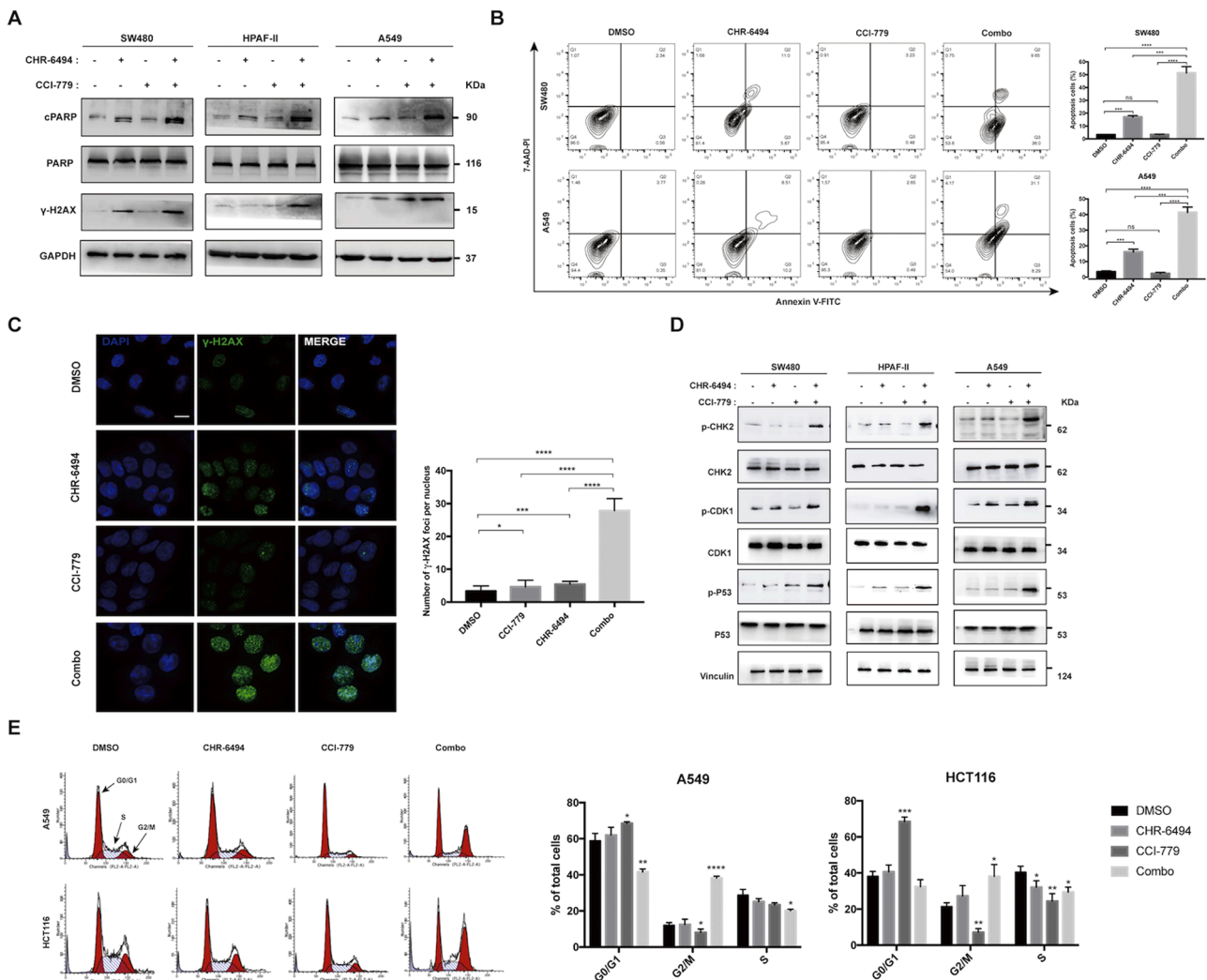


Fig. 4. On-target inhibition of HASPIN and mTOR synergistically trigger enhanced DNA damage and apoptosis in KRAS-mutant cells. (A) The indicated cell lines were exposed to the drugs singly or in combination for 72 h. Representative western blots showing protein levels of γ -H2AX for DNA damage and cPARP for apoptosis induction. (B) Flow cytometry analysis using AnnexinV-FITC and 7AAD-PI was performed after the cells were incubated with CHR-6494, CCI-779, and their combination for 48 h. Representative image of apoptosis induction responding to the treatments determined by flow cytometry analysis (left) and percentage of apoptotic cells (right). (C) Detection of γ -H2AX foci in SW480 cells by immunofluorescence after 72-h treatment with indicated drugs. Representative foci-containing cells at oil 100x objective magnification are shown (left). Mean number of γ -H2AX-focus per SW480 nuclei (right). Over 120 nuclei were analyzed over three experiments. Scale bar: 10 μ m. (D) Expression levels of proteins involved in the DNA damage response pathway of whole protein extract in SW480 cells by western blot analysis after 72-h treatment with indicated drugs. (E) A549 and HCT116 cells were treated with either 600nM CHR-6494, 3 μ M CCI-779, or both for 72 h, and cell-cycle distribution was analyzed by flow cytometry. Left panel: representative images; right panel: statistical analysis of the left panel. Values represent mean \pm SD (n = 3), ns: not significant, * p < 0.05, ** p < 0.01, *** p < 0.001, and **** p < 0.0001.

agent in KRAS-mutant cells, we next examined whether the combination synergistically triggers DNA damage and cell death. Treatment of exponentially proliferating SW480, HPAF-II, and A549 cells for 72-h with CHR-6494 and CCI-779 led to the accumulation of γ -H2AX, a marker for double-stranded DNA breaks (Fig. 4A). Consistent with this finding, we showed significantly elevated γ -H2AX foci in cells treated with both CHR-6494 and CCI-779 by immunofluorescence (Fig. 4C). This triggered the DNA damage response (DDR), as shown by increased phosphorylation of classical DNA damage pathway indicators (P53, CHK2) (Fig. 4D and Supplementary Fig. 3). We next asked if the observed synergistic activity of the combination treatment would result in apoptosis in KRAS-mutant cancer cell lines. Western blot results indicated that the intensity of cleaved PARP (cPARP) signal was markedly enhanced when employing CHR-6494 and CCI-779 in combination (Fig. 4A). Flow cytometry analysis showed that the apoptosis rate in the drug combination-treated cells was higher than that in the HASPIN-treated cells, while no obvious apoptosis was observed in DMSO- or CCI-779-treated cells (Fig. 4B).

We confirmed that CDK1, another DNA damage pathway indicator, was further phosphorylated with dual treatment (Fig. 4D and Supplementary Fig. 3). Phosphorylation of CDK1, resulting in a blockade of mitotic entry [34]. We, therefore, hypothesized that the observed synergistic effect of HASPIN and mTOR inhibitors were associated with a perturbed cell cycle progression. Flow cytometry analysis was performed after the cells were treated with CHR-6494, CCI-779, or their combination, and a significant cell cycle arrest at the G2/M phase was found with combination treatment in A549 and HCT116 cell lines (Fig. 4E). Collectively, these data suggest the enhanced anticancer

activity of combination drug therapy in KRAS-mutant cell lines may due to the more effective induction of apoptosis levels and DNA damage-induced cell cycle arrest.

mTOR cooperatively activates H3T3ph via VRK1 in the context of mutant KRAS

Since the HASPIN or mTOR inhibitor alone inhibits the phosphorylation of histone H3 to a less extent than the combined inhibition, we hypothesized that H3 is the common signaling molecule downstream of both mTOR and HASPIN. As HASPIN and Vaccinia-related kinase 1 (VRK1) are the two major kinases responsible for phosphorylation of H3 [24], we next attempted to clarify whether mTOR regulates histone H3T3ph via a VRK1-dependent manner. The results of real-time PCR and Western blot revealed that inhibition of mTOR down-regulated the expression of VRK1 in A549 and/or SW480 cells (Fig. 5A-B). Inhibiting HASPIN can almost eliminate the phosphorylation of H3 histones (Fig. 5D) in VRK1 knockout SW480 cells (Fig. 5C).

We further examined the relationship between the expression of VRK1 and the KRAS signaling pathway. Two KRAS wild-type cell lines (HT29, H1698) and two KRAS mutant cell lines (SW480, A549) were used in this verification. The results showed that the KRAS mutation caused the activation of mTOR and the expression of VRK1, and the mTOR inhibition partially offset VRK1 expression caused by KRAS mutation (Fig. 5E). VRK1 and H3T3ph expression were up-regulated in KRAS-wildtype HT29 cells overexpressing mutant KRAS-G12V (Fig. 5F-5G), and mTOR suppression partly abrogates this phenomenon (Fig. 5G). In VRK1 knockout SW480 cells, activation of mTOR by

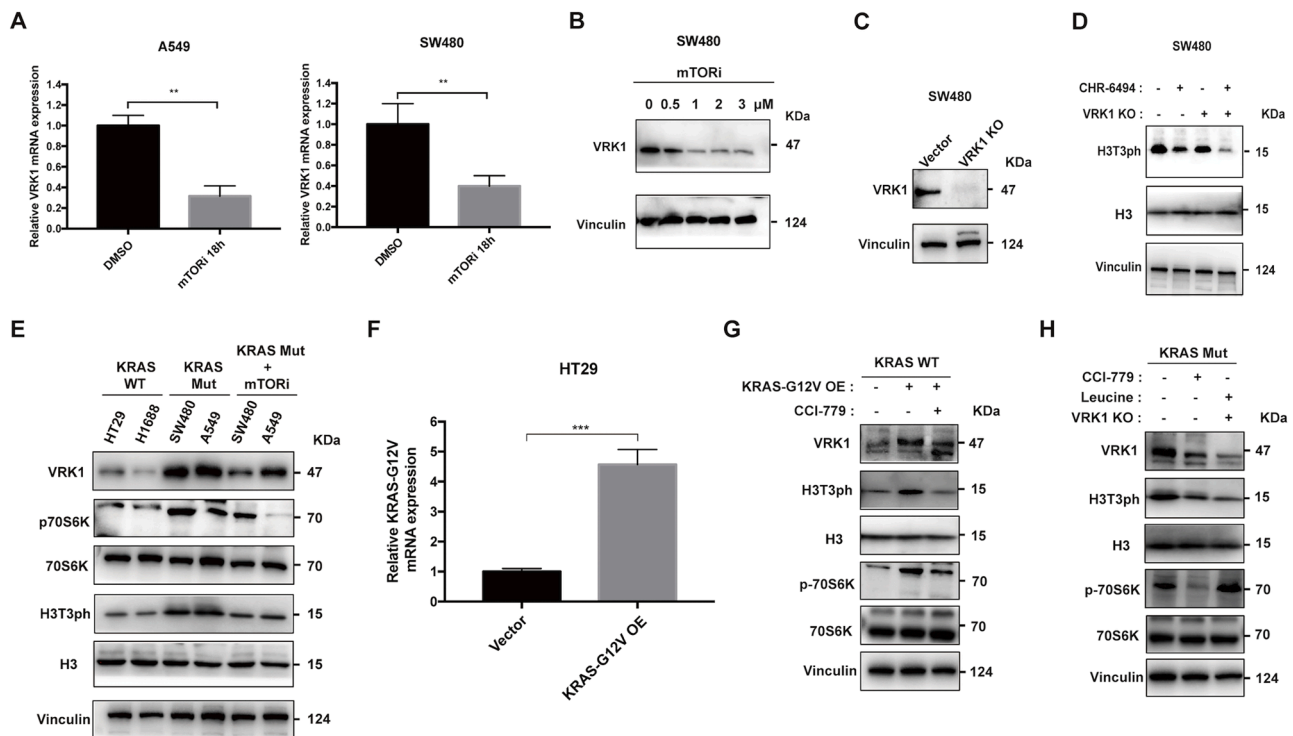


Fig. 5. mTOR cooperatively activates H3T3ph via VRK1 in the context of mutant KRAS.

(A) Effects of mTOR inhibition on mRNA expression of VRK1 in A549 and SW480 cell was examined by real-time PCR. (B) Western blot was used to detect the effect of different concentrations of mTOR inhibition on the expression of VRK1 protein in SW480 cells. (C) Western blots demonstrated VRK1 protein knockout (KO) after treatment with sgRNA in SW480 cells. (D) Detection of H3T3ph protein level by western blot in SW480 cells expressing empty vector control or sgRNA targeting VRK1, untreated or treated with 600nM CHR-6494 for 72 h. (E) Western blots verified the expression level of VRK1 protein and the activity of mTOR signaling pathway in KRAS wild-type cells (KRAS-WT), KRAS mutated cells (KRAS-Mut), and KRAS mutated cells inhibited by mTOR inhibitor CCI-779. (F) Real-time PCR demonstrated the overexpression (OE) of KRAS-G12V mutations in HT29 cells. (G) Western blot analyzed on HT29 cells expressing either empty vector control or KRAS-G12V mutations, untreated or treated with mTOR inhibitor CCI-779 (3 μ M) showed changes in VRK1 and H3T3ph protein levels. (H) Western blot was used to detect the expression of VRK1 and H3T3ph in vector control SW480 cells with CCI-779 treatment or VRK1 KO SW480 cells treated with mTOR activator leucine (3mM). Data are expressed as means \pm SD of the three experiments, ** p < 0.01, *** p < 0.001.

Leucine failed to rescue the level of VRK1 expression and H3T3ph (Fig. 5H). Taken together, our results indicate that KRAS may regulate H3T3ph through the mTOR-VRK1 axis, which is not activated in KRAS wild-type cells.

VRK1-depletion similarly sensitize KRAS-mutant cells to CHR-6494 treatment as mTOR inhibition

As shown above, mTOR affects the phosphorylation of histone H3 by positively regulating the expression of VRK1. Therefore, we concluded that VRK1 depletion can similarly sensitize cells to HASPIN inhibition. Knockout of VRK1 led to a significant dissociation of CPC protein and H3 after CHR-6494 treatment in SW480 cells (Fig. 6B), without affecting the total CPC protein expression (Fig. 6A). In addition, we observed a significant increase in DNA damage (Fig. 6C), apoptosis rate (Fig. 6D), and mitotic catastrophe (Fig. 6E-F) in VRK1-deficient cells treated with CHR-6494. Knockout of VRK1 alone cannot lead to massive dephosphorylation of H3 and cell apoptosis (Figs. 5C and 6D). These results indicate that VRK1 compensates for phosphorylation of H3 when HASPIN is inhibited. Taken together, our results suggest that inhibition of HASPIN potentiates mTOR inhibition by abrogating compensatory phosphorylation of histone H3 (Fig. 6G).

Combined HASPIN/mTOR inhibition causes tumor growth delay in MDA-MB-231 xenografts

We further extended to speculate whether the dual inhibition of HASPIN and mTOR could have a synthetic inhibitory effect on other KRAS-mutant tumors. MDA-MB-231 tumor cells are typical triple-negative breast cancer (TNBC) cells and have KRAS G13D mutations [35]. PTX (paclitaxel) is commonly used as the first-line treatment drug in breast cancer. Unfortunately, the resistance of breast cancer to PTX treatment remain as the leading cause of death associated with treatment failure [36].

Hence, we investigated whether KRAS-mutant MDA-MB-231 cells are sensitive to dual inhibition in vivo. Firstly, when the tumor reached a volume of 50mm³, MDA-MB-231 tumor-bearing mice were grouped ($n = 5$) and administered i.p. with CHR-6494 (50mg/kg), CCI-779 (20mg/kg), CHR-6494/CCI-779, or paclitaxel (20mg/kg). Although no tumor complete regression was observed in any groups with different treatments, tumor growth was significantly retarded in the group with combined CHR-6494 and CCI-779 (Fig. 7A-B). Remarkably, compared with the vehicle control group, paclitaxel monotherapy had no pronounced effect on tumor growth at a dose of 20 mg/kg, which is a relatively high drug treatment concentration (Fig. 7B). The measurement of tumor weight further supported our findings, as the average value was 488.04 ± 117.35 mg for the control group as compared with 313.58 ± 17.64 mg for the CHR-6494 group, 242.8 ± 58.7mg for the CCI-779 group, 118.68 ± 8.75 mg for the combination-treated group, and 339.48 ± 70.8 mg for paclitaxel group (Fig. 7C). No significant difference in body weight was observed in any of the xenograft models after the 21 days of treatment (Fig. 7D), but the mice in the paclitaxel treatment group showed abdominal distension (data not shown). To correlate the in vivo antitumor effects with the above-mentioned mechanisms, DNA damage marker γ -H2AX and cleaved PARP were assessed by Western blot analysis. As shown in Fig. 7E, the combined treatment markedly induced accumulation of γ -H2AX and PARP cleavage in tumors. In summary, these results indicate that the combination of CHR-6494 and CCI-779 inhibition may have potential clinical value in preventing progression of mutant KRAS-driven cancers or cancers with high rate of activation of the mTOR signaling pathway.

Discussion

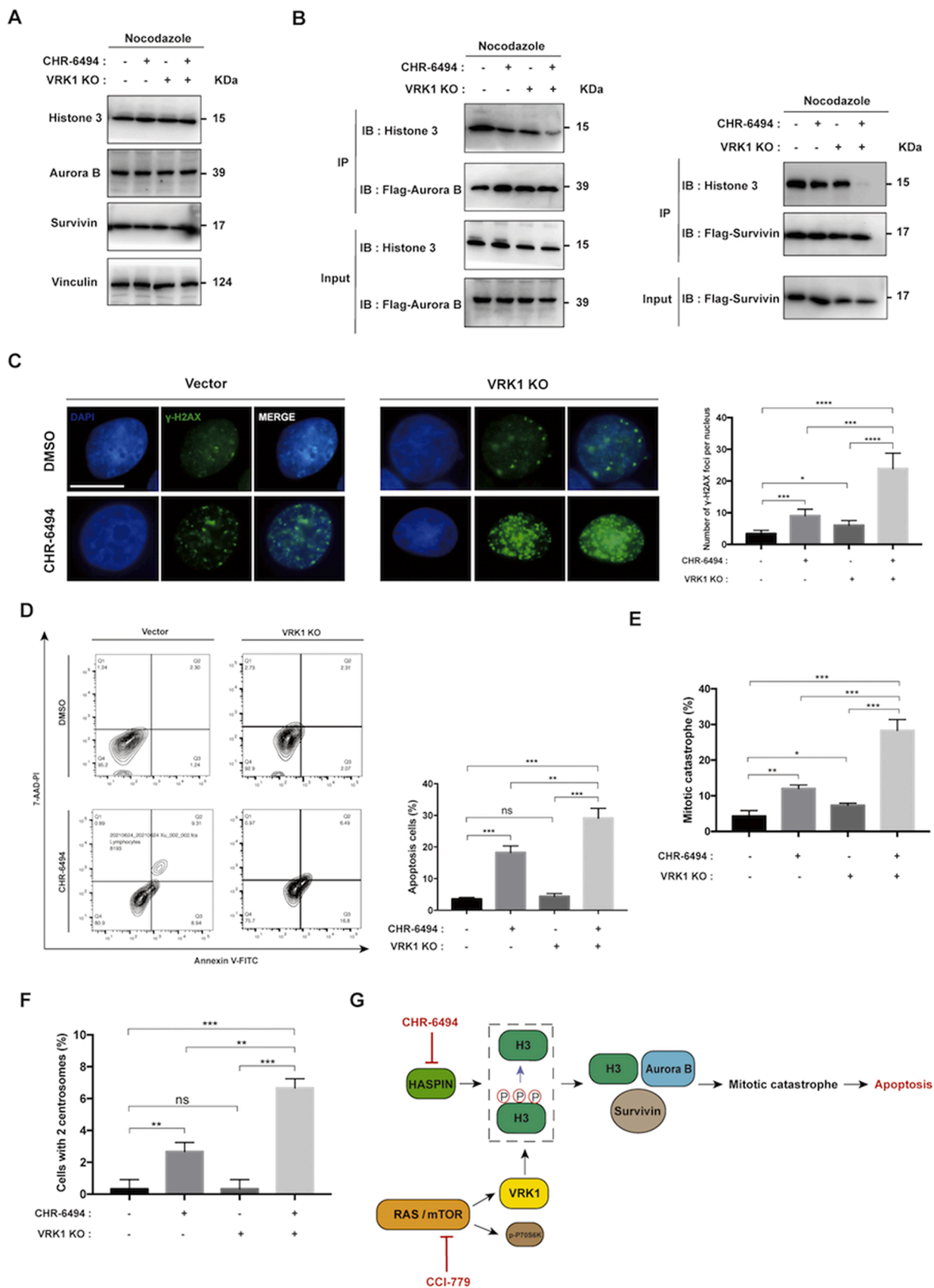
KRAS is the most commonly mutated gene family in cancers [37]. Despite the development of agents that target specific mutations, like

G12C, KRAS-driven cancer remains “untargetable” and is, therefore, a highly lethal disease [1]. Exploiting synthetic lethal interactions to selectively target KRAS-mutant cancers is warranted [37]. In this study, we demonstrated that the combination of CHR-6494 and CCI-779 can synergistically enhance cancer cell death in KRAS-driven cancer cell lines and inhibit tumor growth in xenograft in vivo models. We provide mechanistic evidence that simultaneous inhibition of HASPIN and mTOR signaling allows for more complete disruption of compensatory pathways, resulting in cytotoxic synergy specifically in KRAS-mutant tumors.

HASPIN plays an important role in the regulation of normal mitosis of cells through the regulation of H3 histones. It has been shown that HASPIN inhibitors have potent anti-tumoral effects [24]. HASPIN inhibition leads to the dephosphorylation of the third threonine of H3 histones, which in turn affects the binding of CPC components to histones, and ultimately leads to the disorder of the normal mitotic process of cells. Hence, the main mechanism of HASPIN inhibition leading to tumor cell apoptosis is the occurrence of mitotic catastrophe [29,38]. Consistent with the report, we have shown in our research that a single HASPIN inhibition can also lead to an increase in the rate of tumor cell apoptosis and the probability of mitotic catastrophe (Figs. 3-4). Mitotic catastrophe is the response of mammalian cells to mitotic DNA damage [39]. Studies have confirmed that CPC plays an important role in the process of mitosis, involving many important functions such as spindle formation, chromosome arrangement, sister chromatid separation, spindle checkpoint signaling, and cytokinesis [40]. We reasonably believe that the abnormal positioning of CPC simultaneously causes DNA damage to a certain extent, and then cumulatively leads to the complete disintegration of cells.

The mammalian target of rapamycin (mTOR) regulates cell proliferation, autophagy, and apoptosis by participating in multiple signaling pathways in the body [41]. Inhibition of mTOR/PI3K signaling pathway makes Aurora A-deficient precancerous keratinocytes occur in mitotic catastrophe characterized by multinuclei and polymorphonuclei [42]. The mTORC1 complex components have been shown to be related to mitotic spindles in mouse oocytes [43], and overexpression of mTORC1 leads to impaired spindle formation and aneuploidy [44]. Taken together, these data suggest that mTOR has a regulatory role in cell mitosis. However, how mTOR is involved in regulating the proper cell mitosis process has not been reported. In our study, we found that mTOR inhibition alone could not cause an increase in the number of apoptotic tumor cells, but it enhanced cell death induced by a single HASPIN inhibition (Fig. 4). We also found that combined mTOR inhibition increased the incidence of HASPIN-induced diffused CPC and mitotic catastrophe in tumor cells (Fig. 3). These data suggest that mTOR may be involved in the correct regulation of the cell mitosis process. We reported for the first time that in KRAS-mutant tumors, mTOR is involved in the regulation of VRK1 kinase expression and affects the phosphorylation of H3 histone (Fig. 5), thus coordinating with HASPIN to regulate the correct localization of CPC components during cell mitosis (Fig. 3). Given that VRK1 is a downstream target of mTOR signaling, we verified that depletion of VRK1 expression was sufficient to override CCI-779-mediated potentiation to CHR-6494 (Fig. 6). We consider that in KRAS-mutant tumors, due to the redundancy between mTOR and HASPIN, activation of the mTOR pathway plays a major role in the regulation of H3 phosphorylation in HASPIN-inhibited tumor cells, but the dual inhibition leads to complete dephosphorylation of H3T3ph and ultimately leads to the mitosis catastrophic death in the cell.

Triple negative breast cancer (TNBC) is a highly malignant subtype of breast cancer with a poor prognosis [45]. TNBC accounts for approximately 20% of breast cancer cases. Although conventional chemotherapy regimens have shown some effectiveness in early TNBC cases, in advanced stages the outcome is poor. The PI3K/AKT/mTOR pathway is one of the important and active pathways involved in TNBC chemoresistance and survival. However, PI3K/AKT/mTOR targeted therapy has not been successfully developed for TNBC [46,47]. Here, we



(caption on next page)

Fig. 6. VRK1-depletion similarly sensitize KRAS-mutant cells to CHR-6494 treatment as mTOR inhibition.

(A) Synchronized-treated vector control or VRK1 KO SW480 cells were treated with or without CHR-6494 for 72 h and harvested in mitosis by mechanical shake-off. Western blots showing CPC protein levels (Aurora B and Survivin) and total Histone 3 levels. (B) Detection of the ability of the interaction between CPC protein (Aurora B and Survivin) and Histone 3 by Western blot with immunoprecipitated equal protein of Flag- aurora B (left) and Flag-Survivin (right) in SW480 cells expressing sgRNA targeting VRK1, untreated or treated with CHR-6494 at 600nM. (C) Left: Detection of γ -H2AX by immunofluorescence in SW480 cells expressing sgRNA targeting VRK1, untreated or treated with CHR-6494 at 600nM. Representative foci-containing cells are shown at high power magnification (100x). At least 120 nuclei were analyzed over three experiments. Scale bar: 10 μ m. Right: Statistical analysis of the mean number of γ -H2AX-foci in left. (D) Apoptotic cells detected with AnnexinV/PI staining, and analyzed by flow cytometry in SW480 cells expressing either VRK1 sgRNA or control guide, untreated or treated with 600nM CHR-6494 for three days. Representative images (left) and percentage of apoptotic cells (right) of the apoptosis-inducing response determined by flow cytometry analysis. (E and F) MC and abnormal centrosome amplification were quantitated to SW480 cells expressing either VRK1 sgRNA or control guide, untreated or treated with 600nM CHR-6494. (G) A simplified model showing cross-talk and compensation by mTOR and HASPIN-mediated regulation of H3T3ph. The results are mean \pm SD (n=3), ns: not significant, * p < 0.05, ** p < 0.01, *** p < 0.001, and **** p < 0.0001.

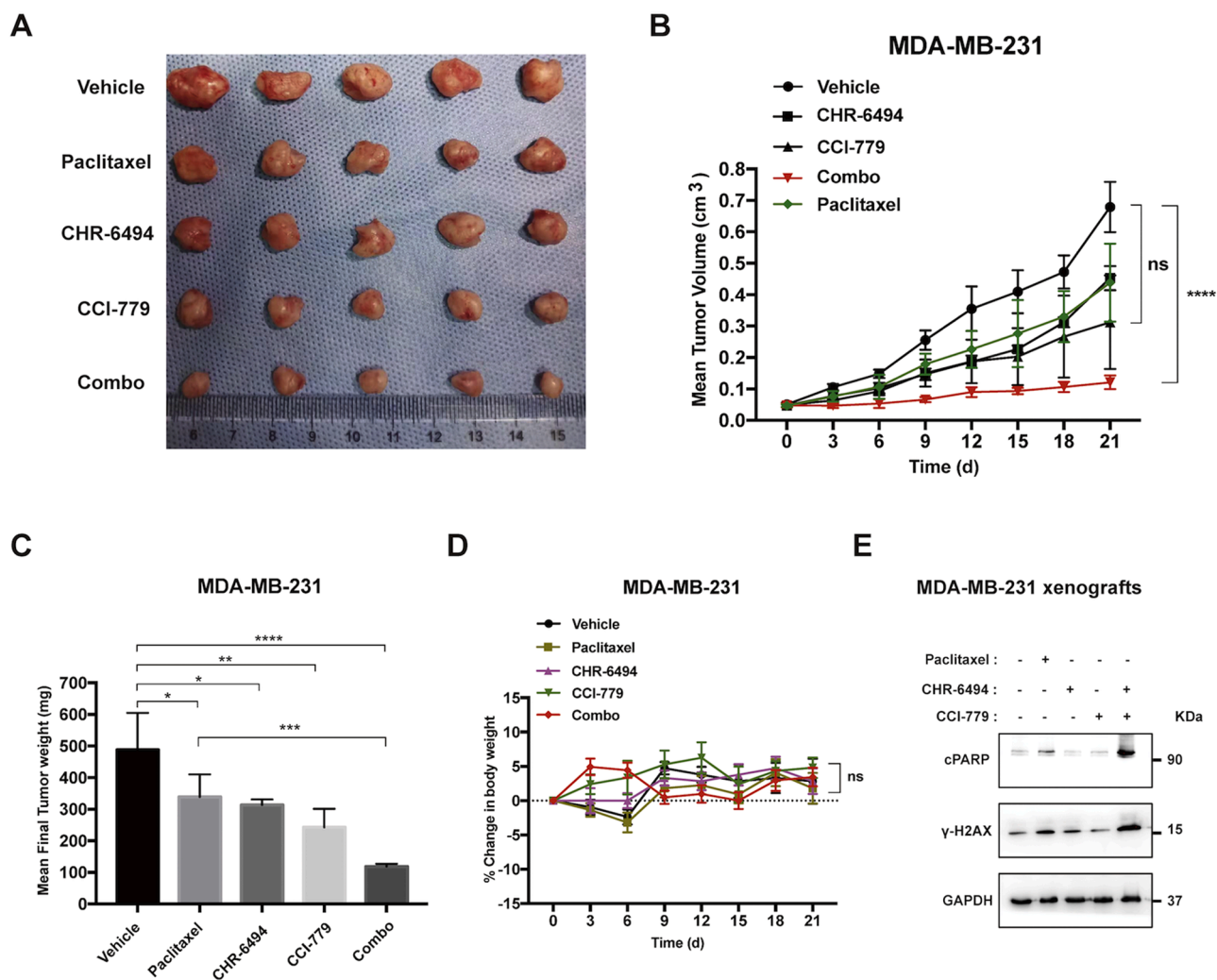


Fig. 7. Combined HASPIN/mTOR inhibition causes tumor growth delay in MDA-MB-231 xenografts.

(A) Representative image of xenografts formed in nude mice using MDA-MB-231 cells exposed to vehicle, CHR-6494, CCI-779, CHR-6494/CCI-779 combination or Paclitaxel. (B) Tumor volume was monitored every three days. (C) Final tumor weight of (A) mentioned tumors at the time of sacrifice. (D) Body-weight changes were measured in tumor-bearing nude mice in each treatment mode. (E) Western blot analysis of changes in protein levels of γ -H2AX and cleaved PARP (cPARP) expression in MDA-MB-231 tumors mentioned in (A). Data represent mean \pm SD (n=3), ns: not significant, * p < 0.05, ** p < 0.01, *** p < 0.001, and **** p < 0.0001.

proved that the combined inhibition of HASPIN/mTOR is more effective than monotherapy and the traditional chemotherapy drug paclitaxel in MDA-MB-231 xenograft tumors. It possible that there is an over-activated mTOR pathway in TNBC, and the mechanism described above exists in cells.

It is noteworthy that apart from KRAS mutations, EGFR and BRAF, which lie upstream and downstream of Kras respectively, are also mutated with high frequency in various tumors. Therefore, whether the synergistic effect of simultaneously inhibiting mTOR and HASPIN can

also be observed in tumor patients harboring EGFR or/and BRAF mutations warrants further investigations.

In summary, the present study is the first to show that CHR-6494 potentiates CCI-779 by abrogating the compensatory phosphorylation pathway of H3 histones, resulting in a synergistic effect in KRAS-mutant tumors. Given the absence of targeted therapies available for KRAS-driven tumors and the high rate of activation of the mTOR signaling pathway in cancers, dual inhibition of mTOR and HASPIN should be investigated as a potential strategy.

Ethics statement

The *in vivo* assay using nude mice was approved by the Experimental Animal Management and Ethics Committee of Fudan University (Project#20180302-003).

Supplementary Fig. 1 HASPIN and mTOR inhibition synergistically suppresses KRAS-mutant cancer cells.

(A) Western blots demonstrated HASPIN protein knockout (KO) after treatment with sgRNA in KRAS-mutant cell lines (SW480 and HCT116) and KRAS-wildtype cell (HT29). (B) Control or cells treated with CCI-779 at indicated concentrations were transfected with sgRNA against HASPIN and assayed for viability after 3 days. Data are expressed as means \pm SD ($n=3$) of the three experiments, ns: not significant, $*p < 0.05$, $**p < 0.01$, $***p < 0.001$ and $****p < 0.0001$.

Supplementary Fig. 2 Combination treatment suppresses HPAF-II tumor xenografted growth

(A) Representative image of xenografts formed in nude mice using HPAF-II cells exposed to indicated drugs. (B) Tumor volume was measured every 3 days after implantation of (A) mentioned tumors. (C) Tumor weight of (A) mentioned tumors 24 days after cell injection. (D) Representative IHC staining images showing the expression of γ -H2AX, Ki-67, and TUNEL in (A) mentioned tumors. (E-G) The percentage of positive γ -H2AX (E), Ki-67 (F), and TUNEL (G) cells in HPAF-II tumor sections were scored at 5 high-power fields ($n=6$ /group). Scale bars: 20 μ m. Data represent mean \pm SD ($n=3$), ns: not significant, $*p < 0.05$, $**p < 0.01$, $***p < 0.001$, and $****p < 0.0001$.

Supplementary Fig. 3 Inhibition of HASPIN and mTOR results in activation of DNA damage pathway

Dual therapy dose- and time-dependently enhanced phosphorylation of CHK2, P53, and CDK1 in SW480 cells after indicated treatment.

CRediT authorship contribution statement

Chenyue Xu: Conceptualization, Methodology, Project administration, Writing – original draft, Writing – review & editing. **Qiongmei Gao:** Conceptualization, Methodology, Project administration, Writing – review & editing. **Zhengming Wu:** Conceptualization, Data curation, Formal analysis. **Weijuan Lou:** Conceptualization, Data curation, Formal analysis. **Xiaoyan Li:** Conceptualization, Data curation, Formal analysis. **Menghui Wang:** Data curation, Formal analysis. **Nianhong Wang:** Validation, Writing – review & editing. **Qingquan Li:** Conceptualization, Resources, Writing – review & editing.

Declaration of Competing Interest

The authors declare that they have no known competing financial interests or personal relationships that could have appeared to influence the work reported in this paper.

Funding

This work was supported by the National Nature Science Foundation of China (NO.81874064). QingQuan Li is a scholar in the National Youth Top-notch Talent Support Program and Program of Shanghai Technology Research Leader (NO.19XD1420100).

Acknowledgments

Not applicable.

Supplementary materials

Supplementary material associated with this article can be found, in the online version, at doi:[10.1016/j.tranon.2022.101540](https://doi.org/10.1016/j.tranon.2022.101540).

References

- [1] D. Uprety, A.A. Adjei, KRAS: From undruggable to a druggable Cancer Target, *Cancer Treat. Rev.* 89 (2020), 102070.
- [2] A.R. Moore, S.C. Rosenberg, F. McCormick, S. Malek, RAS-targeted therapies: is the undruggable drugged? *Nat. Rev. Drug Discov.* 19 (2020) 533–552.
- [3] J.M. Ostrem, U. Peters, M.L. Sos, J.A. Wells, K.M. Shokat, K-Ras(G12C) inhibitors allosterically control GTP affinity and effector interactions, *Nature* 503 (2013) 548–551.
- [4] D.R. Camidge, Y.J. Bang, E.L. Kwak, A.J. Iafrate, M. Varella-Garcia, S.B. Fox, G. J. Riely, B. Solomon, S.H. Ou, D.W. Kim, R. Salgia, P. Fidias, J.A. Engelman, L. Gandhi, P.A. Jänne, D.B. Costa, G.I. Shapiro, P. Lorusso, K. Ruffner, P. Stephenson, Y. Tang, K. Wilner, J.W. Clark, A.T. Shaw, Activity and safety of crizotinib in patients with ALK-positive non-small-cell lung cancer: updated results from a phase I study, *Lancet Oncol.* 13 (2012) 1011–1019.
- [5] C.R. Chong, P.A. Jänne, The quest to overcome resistance to EGFR-targeted therapies in cancer, *Nat. Med.* 19 (2013) 1389–1400.
- [6] A.G. Stephen, D. Esposito, R.K. Bagni, F. McCormick, Dragging ras back in the ring, *Cancer Cell* 25 (2014) 272–281.
- [7] T.E. Stinchcombe, G.L. Johnson, *Lung Cancer* 86 (2014) 121–125.
- [8] F. Skoulidis, L.A. Byers, L. Diao, V.A. Papadimitrakopoulou, P. Tong, J. Izzo, C. Behrens, H. Kadara, E.R. Parra, J.R. Canales, J. Zhang, U. Giri, J. Gudikote, M. A. Cortez, C. Yang, Y. Fan, M. Peyton, L. Girard, K.R. Coombs, C. Toniatti, T. P. Heffernan, M. Choi, G.M. Frampton, V. Miller, J.N. Weinstein, R.S. Herbst, K. K. Wong, J. Zhang, P. Sharma, G.B. Mills, W.K. Hong, J.D. Minna, J.P. Allison, A. Futreal, J. Wang, J.V. Wistuba II, Heymach, Co-occurring genomic alterations define major subsets of KRAS-mutant lung adenocarcinoma with distinct biology, immune profiles, and therapeutic vulnerabilities, *Cancer Discov.* 5 (2015) 860–877.
- [9] H. Hua, Q. Kong, H. Zhang, J. Wang, T. Luo, Y. Jiang, Targeting mTOR for cancer therapy, *J. Hematol. Oncol.* 12 (2019) 71.
- [10] S.Q. Liang, E.D. Bührer, S. Berezowska, T.M. Marti, D. Xu, L. Froment, H. Yang, S. R.R. Hall, E. Vassella, Z. Yang, G.J. Kocher, M.A. Amrein, C. Riether, A. F. Ochsnein, R.A. Schmid, R.W. Peng, mTOR mediates a mechanism of resistance to chemotherapy and defines a rational combination strategy to treat KRAS-mutant lung cancer, *Oncogene* 38 (2019) 622–636.
- [11] A.M. Waters, C.J. Der, KRAS: the critical driver and therapeutic target for pancreatic cancer, *Cold Spring Harb. Perspect. Med.* 8 (2018).
- [12] S.F. Bannoura, M.H. Uddin, M. Nagasaka, F. Fazili, M.N. Al-Hallak, P.A. Philip, B. El-Rayes, A.S. Azmi, Targeting KRAS in pancreatic cancer: new drugs on the horizon, *Cancer Metastasis Rev.* 40 (2021) 819–835.
- [13] L. Buscail, B. Bournet, P. Cordelier, Role of oncogenic KRAS in the diagnosis, prognosis and treatment of pancreatic cancer, *Nat. Rev. Dis. Prim.* 17 (2020) 153–168.
- [14] W.S. Brown, P.C. McDonald, O. Nemirovsky, S. Awrey, S.C. Chafe, D.F. Schaeffer, J. Li, D.J. Renouf, B.Z. Stanger, S. Dedhar, Overcoming adaptive resistance to KRAS and MEK inhibitors by co-targeting mTORC1/2 complexes in pancreatic cancer, *Cell Rep. Med.* 1 (2020), 100131.
- [15] R. Fritsche-Guenther, C. Zasada, G. Mastrobuoni, N. Royle, R. Rainer, F. Roßner, M. Pietzke, E. Klipp, C. Sers, S. Kempa, Alterations of mTOR signaling impact metabolic stress resistance in colorectal carcinomas with BRAF and KRAS mutations, *Sci. Rep.* 8 (2018) 9204.
- [16] J. Moroney, S. Fu, S. Moulder, G. Falchook, T. Helgason, C. Levenback, D. Hong, A. Naing, J. Wheler, R. Kurzrock, Phase I study of the antiangiogenic antibody bevacizumab and the mTOR/hypoxia-inducible factor inhibitor temsirolimus combined with liposomal doxorubicin: tolerance and biological activity, *Clin. Cancer Res.* 18 (2012) 5796–5805.
- [17] J. Tabernero, F. Rojo, E. Calvo, H. Burris, I. Judson, K. Hazell, E. Martinelli, S. Ramon y Cajal, S. Jones, L. Vidal, N. Shand, T. Macarulla, F.J. Ramos, S. Dimitrijevic, U. Zoellner, P. Tang, M. Stumm, H.A. Lane, D. Lebowitz, J. Baselga, Dose- and schedule-dependent inhibition of the mammalian target of rapamycin pathway with everolimus: a phase I tumor pharmacodynamic study in patients with advanced solid tumors, *J. Clin. Oncol.* 26 (2008) 1603–1610.
- [18] N.D. Trivedi, S. Armstrong, H. Wang, M. Hartley, J. Deeken, A. Ruth He, D. Subramaniam, H. Melville, C. Albanese, J.L. Marshall, J. Hwang, M.J. Pishvaian, A phase I trial of the mTOR inhibitor temsirolimus in combination with capecitabine in patients with advanced malignancies, *Cancer Med.* 10 (2021) 1944–1954.
- [19] I.Z. Uras, H.P. Moll, E. Casanova, Targeting KRAS mutant non-small-cell lung cancer: past, present and future, *Int. J. Mol. Sci.* 21 (2020).
- [20] K. Ng, J. Tabernero, J. Hwang, E. Bajetta, S. Sharma, S.A. Del Prete, E. R. Arrowsmith, D.P. Ryan, M. Sedova, J. Jin, K. Malek, C.S. Fuchs, Phase II study of everolimus in patients with metastatic colorectal adenocarcinoma previously treated with bevacizumab-, fluoropyrimidine-, oxaliplatin-, and irinotecan-based regimens, *Clin. Cancer Res.* 19 (2013) 3987–3995.
- [21] K.L. Spindler, M.M. Sorensen, N. Pallisgaard, R.F. Andersen, B.M. Havelund, J. Ploen, U. Lassen, A.K. Jakobsen, Phase II trial of temsirolimus alone and in combination with irinotecan for KRAS mutant metastatic colorectal cancer: outcome and results of KRAS mutational analysis in plasma, *Acta Oncol.* 52 (2013) 963–970.
- [22] T. Tian, X. Li, J. Zhang, mTOR signaling in cancer and mTOR inhibitors in solid tumor targeting therapy, *Int. J. Mol. Sci.* (2019) 20.
- [23] F. Wang, J. Dai, J.R. Daum, E. Niedzialkowska, B. Banerjee, P.T. Stukenberg, G. J. Gorbosky, J.M. Higgins, Histone H3 Thr-3 phosphorylation by Haspin positions Aurora B at centromeres in mitosis, *Science* 330 (2010) 231–235.

- [24] N.G. Amoussou, A. Bigot, C. Roussakis, J.H. Robert, Haspin: a promising target for the design of inhibitors as potent anticancer drugs, *Drug Discov. Today* 23 (2018) 409–415.
- [25] J.M. Higgins, Haspin: a newly discovered regulator of mitotic chromosome behavior, *Chromosoma* 119 (2010) 137–147.
- [26] J. Dai, A.V. Kateneva, J.M. Higgins, Studies of haspin-depleted cells reveal that spindle-pole integrity in mitosis requires chromosome cohesion, *J. Cell Sci.* 122 (2009) 4168–4176.
- [27] M. Platani, L. Trinkle-Mulcahy, M. Porter, A.A. Jayaprakash, W.C. Earnshaw, Mio depletion links mTOR regulation to Aurora A and Plk1 activation at mitotic centrosomes, *J. Cell Biol.* 210 (2015) 45–62.
- [28] S.H. Choi, T.F. Martinez, S. Kim, C. Donaldson, M.N. Shokhirev, A. Saghatelian, K. A. Jones, CDK12 phosphorylates 4E-BP1 to enable mTORC1-dependent translation and mitotic genome stability, *Genes Dev.* 33 (2019) 418–435.
- [29] J.C. Melms, S. Vallabhaneni, C.E. Mills, C. Yapp, J.Y. Chen, E. Morelli, P. Waszyk, S. Kumar, D. Deming, N. Moret, S. Rodriguez, K. Subramanian, M. Rogava, A.N. R. Cartwright, A. Luoma, S. Mei, T.J. Brinker, D.M. Miller, A. Spektor, D. Schadendorf, N. Riggi, K.W. Wucherpennig, P.K. Sorger, B. Izar, Inhibition of haspin kinase promotes cell-intrinsic and extrinsic antitumor activity, *Cancer Res.* 80 (2020) 798–810.
- [30] T.C. Chou, Drug combination studies and their synergy quantification using the Chou-Talalay method, *Cancer Res.* 70 (2010) 440–446.
- [31] A.E. Kelly, C. Ghenoiu, J.Z. Xue, C. Zierhut, H. Kimura, H. Funabiki, Survivin reads phosphorylated histone H3 threonine 3 to activate the mitotic kinase Aurora B, *Science* 330 (2010) 235–239.
- [32] F. Wang, N.P. Ulyanova, M.S. van der Waal, D. Patnaik, S.M. Lens, J.M. Higgins, A positive feedback loop involving Haspin and Aurora B promotes CPC accumulation at centromeres in mitosis, *Curr. Biol.* 21 (2011) 1061–1069.
- [33] M. Nitta, O. Kobayashi, S. Honda, T. Hirota, S. Kuninaka, T. Marumoto, Y. Ushio, H. Saya, Spindle checkpoint function is required for mitotic catastrophe induced by DNA-damaging agents, *Oncogene* 23 (2004) 6548–6558.
- [34] J.A. Ubersax, E.L. Woodbury, P.N. Quang, M. Paraz, J.D. Blethrow, K. Shah, K. M. Shokat, D.O. Morgan, Targets of the cyclin-dependent kinase Cdk1, *Nature* 425 (2003) 859–864.
- [35] A. Tiwari, M. Iida, C. Kosnopfel, M. Abbariki, A. Menegakis, B. Fehrenbacher, J. Maier, M. Schaller, S.Y. Brucker, D.L. Wheeler, P.M. Harari, U. Rothbauer, B. Schitteck, D. Zips, M. Toulany, Blocking Y-Box binding protein-1 through simultaneous targeting of PI3K and MAPK in triple negative breast cancers, *Cancers* 12 (2020).
- [36] V.M. Dan, R.S. Raveendran, S. Baby, Resistance to intervention: paclitaxel in breast cancer, *Mini Rev. Med. Chem.* 21 (2021) 1237–1268.
- [37] A.J. Aguirre, W.C. Hahn, Synthetic lethal vulnerabilities in KRAS-mutant cancers, *Cold Spring Harb. Perspect. Med.* 8 (2018).
- [38] F. Wang, N.P. Ulyanova, J.R. Daum, D. Patnaik, A.V. Kateneva, G.J. Gorbsky, J. M. Higgins, Haspin inhibitors reveal centromeric functions of Aurora B in chromosome segregation, *J. Cell Biol.* 199 (2012) 251–268.
- [39] X. Huang, T. Tran, L. Zhang, R. Hatcher, P. Zhang, DNA damage-induced mitotic catastrophe is mediated by the Chk1-dependent mitotic exit DNA damage checkpoint, *Proc. Nat. Acad. Sci. U.S.A.* 102 (2005) 1065–1070.
- [40] M. Carmena, M. Wheelock, H. Funabiki, W.C. Earnshaw, The chromosomal passenger complex (CPC): from easy rider to the godfather of mitosis, *Nat. Rev. Mol. Cell Biol.* 13 (2012) 789–803.
- [41] Z. Zou, T. Tao, H. Li, X. Zhu, mTOR signaling pathway and mTOR inhibitors in cancer: progress and challenges, *Cell Biosci.* 10 (2020) 31.
- [42] W.K. Ryan, J. Fernandez, M.K. Peterson, D.W. Sheneman, B.K. Podell, S. De, E. C. Torchia, Activation of S6 signaling is associated with cell survival and multinucleation in hyperplastic skin after epidermal loss of AURORA-A Kinase, *Cell Death Differ.* 26 (2019) 548–564.
- [43] Y. Kogasaka, Y. Hoshino, Y. Hiradate, K. Tanemura, E. Sato, Distribution and association of mTOR with its cofactors, raptor and rictor, in cumulus cells and oocytes during meiotic maturation in mice, *Mol. Reprod. Dev.* 80 (2013) 334–348.
- [44] A. Astrinidis, W. Senapedis, E.P. Henske, Hamartin, the tuberous sclerosis complex 1 gene product, interacts with polo-like kinase 1 in a phosphorylation-dependent manner, *Hum. Mol. Genet.* 15 (2006) 287–297.
- [45] J. Sukumar, K. Gast, D. Quiroga, M. Lustberg, N. Williams, Triple-negative breast cancer: promising prognostic biomarkers currently in development, *Expert Rev. Anticancer Ther.* 21 (2021) 135–148.
- [46] R.L.B. Costa, H.S. Han, W.J. Gradishar, Targeting the PI3K/AKT/mTOR pathway in triple-negative breast cancer: a review, *Breast Cancer Res. Treat.* 169 (2018) 397–406.
- [47] M.A. Khan, V.K. Jain, M. Rizwanullah, J. Ahmad, K. Jain, PI3K/AKT/mTOR pathway inhibitors in triple-negative breast cancer: a review on drug discovery and future challenges, *Drug Discov. Today* 24 (2019) 2181–2191.